COMPARISON OF TRANSDUCING END-STOPS WITH DIFFERENT STIFFNESS IN MEMS ELECTROSTATIC ENERGY HARVESTERS

Cuong. P. Le[1*], Einar Halvorsen[1], Oddvar Søråsen[2], and Eric. M. Yeatman[3]
[1]Department of Micro and Nano Systems Technology, Vestfold University College, Horten, Norway
[2]Department of Informatics, University of Oslo, Oslo, Norway
[3]Department of Electrical and Electronic Engineering, Imperial College London, UK

Abstract: This paper presents experiments on electrostatic energy harvesters with different designs of end-stop transducers, giving output power improvement and bandwidth enhancement under displacement-constrained operation. The end-stops function as additional electrostatic transducers collecting additional power from internal impacts. We investigate the influence of end-stop stiffness on output power by comparing two devices with different end-stop stiffness. The comparison shows that the compliant end-stops result in higher output power than the stiff end-stops do and increase the acceleration-amplitude range where transducing end-stops are beneficial. Compared to their linear response, the two variants enlarge the 3dB-bandwidth with factors up to 15.9 and 13.7 respectively.

Keywords: electrostatic energy harvester, impacts, end-stops and stiffness

INTRODUCTION

Typical vibration energy harvesters are spring-mass systems converting from mechanical to electrical energy using one of the three main conversion mechanisms: electromagnetic, piezo-electric or electrostatic. For practical harvesters with high mechanical quality factor, *Q,* or with limited space for proof mass motion, end-stop designs need to be integrated into the system to limit the proof mass motion in a controlled way. Typical effects of conventional end-stops have been reported for many prototypes [1-4], resulting in enlargement of bandwidth, but with saturation of output power. Recent harvester devices have been designed to utilize a large proof mass having impact on piezoelectric end-stops [5-7]. The power can then be extracted from stress variations of the piezoelectric cantilevers.

The saturated output power due to increasing acceleration means that harvester efficiency is reduced. In order to overcome this drawback, we propose a concept of microscale impact devices that utilize the end-stops as additional (secondary) transducers to harvest extra power when the main (primary) transducers reach the saturated output level. All transducers are designed using electrostatic conversion and are compactly fitted within the same die. The fundamental performance of the impact devices were presented in our own previous studies [8-9]. However, the results showed that for the secondary output power to be substantial, the acceleration had to be increased significantly beyond the level required for end-stop impacts to commence. Consequently, there is an acceleration gap without any benefit of the transducing end-stops. Our previous transducing end-stops were relatively stiff. In the current work, we investigate the effect of making the end-stop structures more compliant. Therefore, the secondary transducers are expected to be activated at smaller excitation levels and give higher output powers than the stiffer ones.

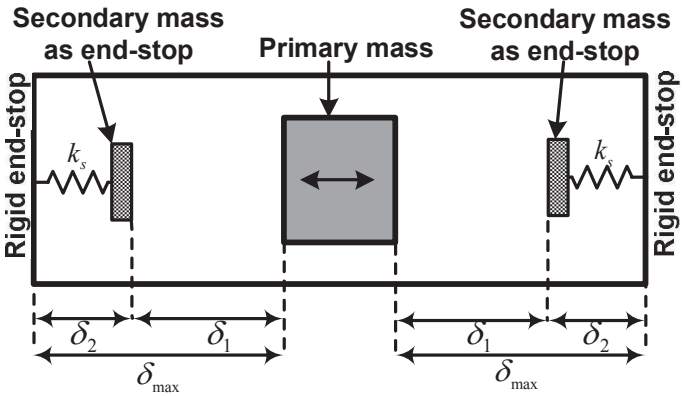

Fig. 1: Schematic of the device concept with end-stop transducers.

DEVICE PRINCIPLE AND DESCRIPTION

Figure 1 illustrates the design principle of the impact devices with their displacement limits. The maximum proof mass displacement in the primary structure is δ_{max}. The secondary structures function as end-stops when the primary proof mass approaches the limit. The distance from the primary mass to the secondary mass is δ_1 from the equilibrium position. The possible displacement range of the secondary proof masses is then $\delta_2=\delta_{max}-\delta_1$. The extra output power from the secondary transducers is obtained

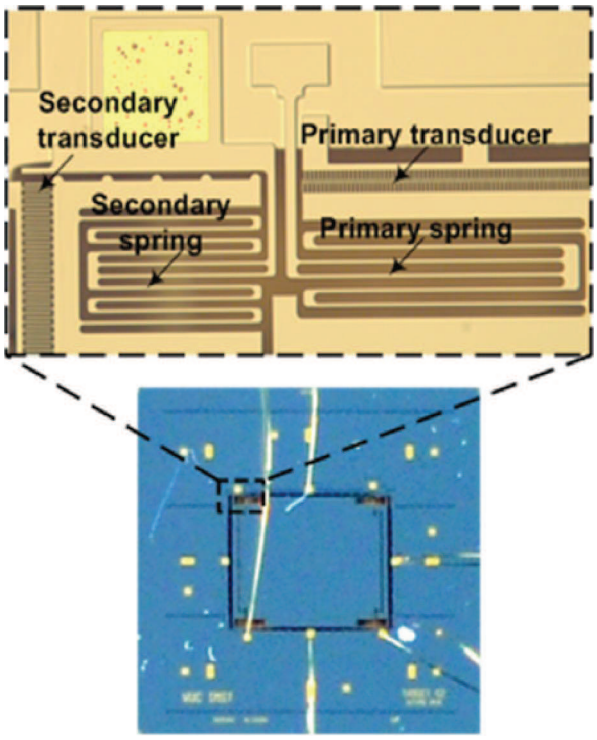

Fig. 2: A picture of impact device fabricated in MEMSCAP MPW using the SOIMUMPs process with device layer thickness of 25µm and secondary/primary spring structures.

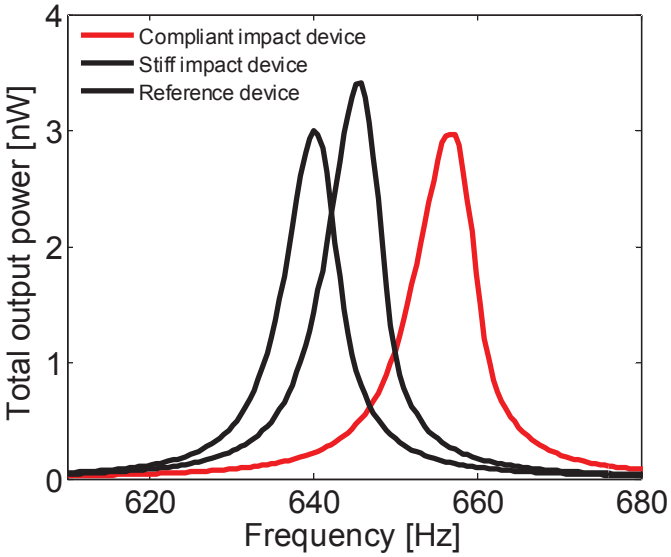

Fig. 3: Comparison of measured frequency responses: reference device with k_s=0N/m, stiff impact device with k_s=21.2N/m and compliant impact device with k_s=16.3N/m at a small acceleration A=0.05g and V_b=12V.

when the primary-mass displacement exceeds δ_1 and is additional to the power from the primary transducers. At a given excitation level within this impact regime, the output power of the secondary transducers significantly depends on the compliance of the secondary structures. In order to investigate this aspect, we compare two impact designs with different secondary structures, henceforth referred to as the stiff and the compliant impact device respectively. Their performances are compared to a reference device with the same die dimension, the same maximum displacement δ_{max}, but without the secondary structures.

Figure 2 shows the device fabricated in the SOIMUMPS process with 25µm-thickness. The impact device consists of two-stage transducers: the primary structure with a large-area mass and an overlap-varying comb transducer, and two secondary structures with gap-closing transducers functioning as end-stops. The area ratio of the primary and secondary structures is 11.5. The active device area is 4×5 mm^2 and the maximum displacement is δ_{max}=10µm. Further details of the device concept design are given in [8-9].

The only difference between the two impact-devices lies in the mechanical stiffness of the transducing end-stops. In particular, the stiffness of the primary device and all transducer capacitor designs are equal. The primary device stiffness is k_p=18.2N/m. The end-stop stiffness is k_s=21.2N/m for the stiff impact device and k_s=16.3N/m for the compliant impact device. The three devices were designed to achieve the same resonant frequencies, but over-etching on the springs during fabrication caused a deviation of about 1.3%.

MEASUREMENT RESULTS

Each device is glued onto a chip carrier, mounted onto a printed circuit board and connected to buffer amplifiers and further data acquisition equipment. A resistive load R_L for evaluating output power is connected across each electrical port. The devices are horizontally shaken by a TIRA vibratory exciter and the input/output signals are controlled using National Instruments' LabView. The Precision Impedance Analyzer 4249A 40Hz-110MHz, Agilent Technologies, is used to analyze the impedance of the primary and reference transducers. The magnitude of the impedance as a function of frequency has a minimum at the resonance and a maximum at the anti-resonance. The minimum value was selected for the resistive load R_L [10]. The values are R_L=21.5MΩ and R_L=14.8MΩ for the impact and reference devices respectively. The total output power of the impact device is obtained by adding the primary and secondary output powers obtained from logging the voltage across the known resistors.

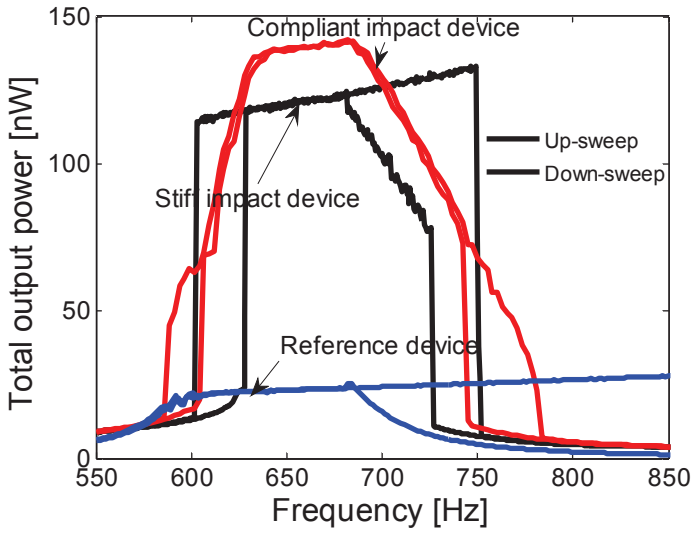

Figure 4. Performance comparison of measured frequency responses for three devices in up-down sweeps at a high acceleration A=2.15g and V_b=12V.

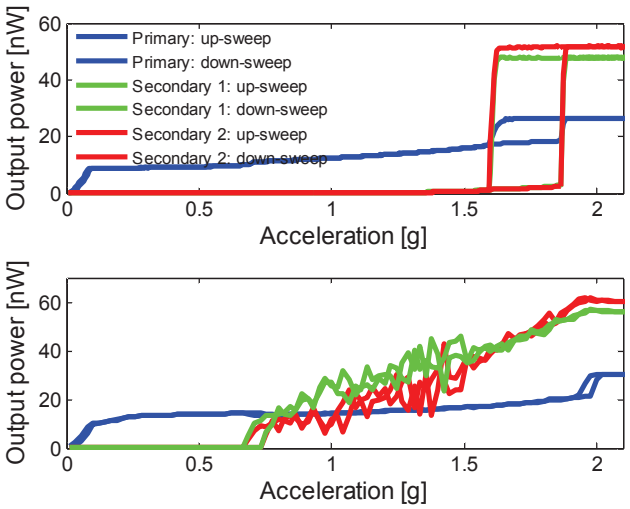

Figure 5. Measured acceleration responses in up-down sweeps at their resonant frequencies and V_b=12V for two devices: stiff impact device (top) and compliant impact device (bottom).

Figure 3 shows comparison of measured frequency responses for three devices at a small acceleration A=0.05g. The different resonant frequencies are caused by the fabrication spread mentioned before. At this vibrating level, the total output power of the impact devices is completely dominated by the primary transducers. Therefore, the output power of the reference device is slightly higher than those of the impact devices when no impact occurs. At resonant frequency, the total output power of the impact devices is 3.0nW while this value is of 3.4nW for the reference device.

Measured frequency responses are compared at a higher acceleration A=2.15g as shown in Figure 4. This acceleration is sufficient to drive the proof mass displacement to the limit, introducing frequent impacts on the end-stops. The reference device has conventional end-stops and displays well known phenomena such as frequency hysteresis and the jump phenomenon on the high-frequency side of the response. The output power of the reference device reaches a saturated level P=23.6nW when the displacement amplitude is maximum δ_{max}. For the impact devices, the primary mass hits the secondary masses at the relative position δ_1 and then activates the secondary transducers through the impact force between the masses. The extra output power converted by the secondary transducers contributes to a much higher total output power than that of the reference device. Near the resonant frequency, the total power P=140nW of the compliant impact device is also larger than the P=127nW of the stiff impact device. The compliant device has a 3dB-bandwidth of 42.0Hz, comparing favorably to the 124.4Hz of the stiff device. The measured results also display that the compliant device gives a reduced frequency hysteresis in comparison to that of the stiff device.

Figure 5 shows acceleration responses of both impact devices in up- and down-sweeps at their resonant frequencies and V_b=12V. Both primary masses begin to hit the transducing end-stops at an acceleration amplitude A=0.09g, giving primary power of 8.7nW. Then, their primary power levels rise slowly with further increase of A. The measured results show that the primary power of both impact devices are comparable for A>0.09g. The stiff impact device gives a saturated primary power of P=26.4nW for A>1.87g in the up-sweep and A>1.59g in the down-sweep. The slightly bigger value of P=30.4nW is found for the compliant impact device for A>1.95g in both sweeps. The stiff impact device delivers significant secondary power above A=1.59g, saturating at P=51.7nW. For the compliant impact device, the secondary transducer output becomes appreciable already at A=0.73g. Increase of the secondary outputs is then approximately proportional to the acceleration until it levels off at P=60.8nW for A>1.95g. Furthermore, the compliant device exposes an acceleration hysteresis significantly narrower than the stiff device does.

The total output powers of the three devices are compared to of their measured acceleration response as shown in Figure 6. The outputs from the transducing end-stops result in a total output power of the compliant impact-device becoming higher than that of the reference device for A=0.78g, while this

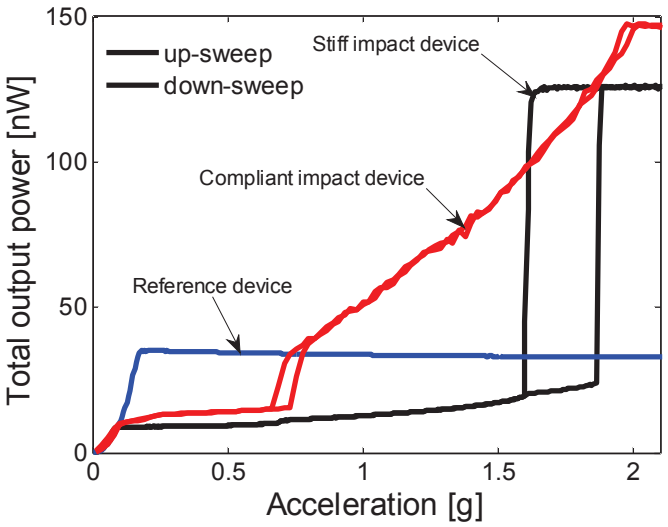

Figure 6. Performance comparison of measured acceleration responses for three devices in up-down sweeps at their resonant frequencies and V_b=12V.

value is about 2 times higher for the stiff impact device. For sufficient accelerations, the stiff and compliant impact devices have total output powers about 5 and 6 times higher than that of the reference device respectively. The compliant end-stops show that the output power is growing roughly linearly with regard to the acceleration before the saturation is reached, while the stiff end-stops exhibit a jump phenomenon.

CONCLUSION

Impact devices with different stiffness on the transducing end-stops were investigated for possible improvement of the output power and the bandwidth when the proof mass displacement is accelerated to the limit points. The most compliant impact device exhibited significant power from secondary transducers at about half the acceleration amplitude necessary for exciting the secondary transducers in the stiff impact device. Hence the choice of end-stop stiffness has dramatic consequences for the size of the acceleration gap in these devices. Both types of the impact devices give much greater maximum power, by a factor 5-6, than the reference device with the conventional end-stops constrained by the same maximum displacement amplitude δ_{max}. Further improvements will be sought by making end-stops transducers more effective at small actuation distances.

ACKNOWLEDGEMENT

This work was financially supported by the Research Council of Norway under grant 191282.

REFERENCES

[1] Soliman M. S. M., Abdel-Rahman E. M., El-Saadany E. F., Mansour R. R. 2008 A wideband vibration- based energy harvester *J. Micromech. Microeng.* 18:115021

[2] Hoffmann D., Folkmer B., Manoli Y. 2009 Fabrication, characterization and modeling of electrostatic micro-generators *J. Micromech. Microeng.* 19:094001

[3] Blystad L-C. J., Halvorsen E., Husa S. 2010 Piezoelectric MEMS energy harvesting driven by harmonic and random vibrations *IEEE Trans. Ultr. Ferr. Freq. Contr.* 57:908-919

[4] Liu H., Tay C. J., Quan C., Kobayashi T., Lee C. 2011 Piezoelectric MEMS energy harvester for low-frequency vibrations with wideband operation range and steadily increased output power *J. Microelectromech. Syst.* 20:1131-1142.

[5] Umeda M., Nakamura K., Ueha S. 1997 Energy storage characteristics of a piezo-generator using impact induced vibration *Jpn. J. Appl. Phys.* 36:3146–3151

[6] Moss S., Barry A., Powlesland I., Galea S., Carman G. P. 2011 A broadband vibro-impacting power harvester with symmetrical piezoelectric bimorph-stops *J. Smart Mat. Struct.* 20:045013

[7] Gu L., Livermore C. 2011 Impact-driven, frequency up-converting coupled vibration energy harvesting device for low frequency operation *J. Smart Mat. Struct.* 20:045004

[8] Le C. P., Halvorsen E., Søråsen O., Yeatman E. M. 2011 An electrostatic energy harvester with power-extracting end stops driven by wideband vibrations *Technical Digest PowerMEMS 2011 (Seoul, Korea, 15-18 November 2011)* 122-125

[9] Le C. P., Halvorsen E., Søråsen O., Yeatman E. M. 2012 Microscale electrostatic energy harvester using internal impacts *J. Int. Mat. Syst. Struct.* 23:1409-1421

[10] Lei A., Xu R., Thyssen A., Stoot A. C., Christiansen T. L., Hansen K., Lou-Møller R., Thomsen E. V., Birkelund K. 2011 MEMS-based thick film PZT vibrational energy harvester *Proc. IEEE Int. Conf. Micro Electro Mech. Syst. 2011 (Cancun, Mexico, 23-27 January 2011)* 125-128